Journal of Biomedical Optics

BiomedicalOptics.SPIEDigitalLibrary.org

Dermal fiber structures and photoaging

Jimmy Le Digabel
Sophia Houriez-Gombaud-Saintonge
Jérôme Filiol
Christophe Lauze
Gwendal Josse

SPIE.

Jimmy Le Digabel, Sophia Houriez-Gombaud-Saintonge, Jérôme Filiol, Christophe Lauze, Gwendal Josse, "Dermal fiber structures and photoaging," *J. Biomed. Opt.* **23**(9), 096501 (2018), doi: 10.1117/1.JBO.23.9.096501.

Dermal fiber structures and photoaging

Jimmy Le Digabel,* Sophia Houriez-Gombaud-Saintonge, Jérôme Filiol, Christophe Lauze, and Gwendal Josse
Pierre Fabre Dermo Cosmétique, Clinical Research Center, Toulouse, France

Abstract. The use of multiphoton imaging has become a standard technique to visualize the dermis fibers as it requires no specific staining. The density and organization of collagen and elastin are common markers of skin intrinsic aging and photoaging; thus, there is a need of grading this skin aging with quantitative indicators able to provide a robust evaluation of the dermis fibers' state. We propose a systematic analysis of multiphoton images of skin biopsies taken on the buttock and the forearm of patients of different ages. The intensity histograms of images were analyzed through their moments, a wavelet decomposition was done, and the wavelet coefficients distribution was fitted by a generalized Gaussian distribution. Different parameters relative to the collagen or elastin densities, organizations, and structures were calculated and exhibit phenomena specific to intrinsic or extrinsic aging. Those indicators could become a standard method to analyze the degree of skin aging (intrinsic or extrinsic) through multiphoton imaging. [DOI: 10.1117/1.JBO.23.9.096501]

Keywords: multiphoton; image analysis; skin aging.

Paper 180135RR received Mar. 7, 2018; accepted for publication Aug. 29, 2018; published online Sep. 22, 2018.

1 Introduction

Skin aging results from intrinsic biological mechanisms and from extrinsic factors, such as sun exposure. These two types of skin aging exhibit different clinical characteristics, suggesting they correspond to different mechanisms: intrinsically aged skin is characterized by fine wrinkling, a smooth texture, and a gradual loss of elasticity; extrinsically aged skin is characterized by coarse wrinkling, a roughened texture, and a marked loss of elasticity.[1]

Multiphoton microscopy has become an important tool to visualize dermal fibers, as it does not require any specific staining. Second-harmonic generation (SHG) and autofluorescence (AF) are the two phenomena that enable the visualization of the dermal fibers. More precisely, collagen fibers are known to have a strong SHG response,[2] whereas elastin provides most of the AF signal in the dermis.[3]

To quantify skin aging, an SHG-to-AF dermal aging index (SAAID) was proposed.[4] This parameter has been proven to be relevant for intrinsic and extrinsic aging analyses.[5] However, the SAAID calculation combines both SHG and AF signals; therefore, it is not possible to determine if changes in SAAID scores are mostly due to changes in collagen or elastin. The elastin-to-collagen ratio has also been proposed to quantify skin aging using collagen and elastin densities instead of their signals' intensities.[6] This parameter appeared more precise than the SAAID score for measuring skin aging, but it still did not provide independent information on the different dermal components. Some studies aimed to analyze collagen and elastin independently.[7] However, as these only considered the SHG and AF mean intensities, no information on the matrix structure and its organization could be obtained.

The organization of the collagen network of the dermis or of other tissues has been analyzed with several methods: gray-level co-occurrence matrix analysis,[8] fast Fourier transform analysis,[9] or fiber extraction algorithms.[10] Some of the approaches have tended to analyze the main orientation of the fibers in the images. But these methods have not yet been used for studying the aging of the human dermis. The elastin network can be qualitatively analyzed through histopathology.[11] Specifically, solar elastosis appears as a clear disorganization of the elastin fiber network, easily seen on photodamaged skin. Its severity can be scored on histological slides.[12] But this approach needs a specific staining procedure and can be operator dependent. AF imaging by multiphoton microscopy leads to a more precise visualization of the elastin network[13] with no need for staining.

In this work, punch biopsies were performed on the buttock and on the exterior forearm of healthy patients of different ages to study the effects of intrinsic and extrinsic aging. Indeed, the exterior forearm is a chronically UV-exposed area compared to the buttock, and it may combine effects of intrinsic and photoaging. As SHG and AF provide natural contrast, multiphoton images of the reticular dermis were acquired on thin biopsy sections (50 μm) with no previous treatment. First, the pixel intensity distributions of the three-dimensional (3-D) images were analyzed using different parameters. Then, a Daubechies[14] wavelet transform of the images was performed and the distribution coefficients were modeled by a generalized Gaussian distribution (GGD), this distribution being known to capture the statistical properties of wavelet images.[15,16]

2 Methods

2.1 *Clinical Study*

This study was conducted in Toulouse, France, in accordance with the Declaration of Helsinki and was approved by the "Comité de Protection des Personnes Sud-Ouest et Outre Mer III" (ref.: 2014/44). Seven healthy volunteers aged between 20 and 30 years old and seven healthy volunteers aged 60 and older were recruited. The older subject group presented

*Address all correspondence to: Jimmy Le Digabel, E-mail: jimmy.le.digabel@pierre-fabre.com

a photoaging score SCINEXA (score of intrinsic and extrinsic skin aging)[17] superior or equal to 2, proving clear photoaging. All participants gave written informed consent before taking part in the study.

2.2 *Skin Samples*

Four millimeters punch biopsies of sun-protected buttock and sun-exposed dorsal forearm skin were performed on each subject. Samples were immediately included in optimal cutting temperature compound and frozen in liquid nitrogen. Thin sections (50 μm) were fixed with acetone for 10 min and mounted between a microscope slide and a coverslip with a mounting medium (Dako, ref S3023).

2.3 *Multiphoton Microscopy Images*

Image acquisition was performed on a Nikon A1-MP-Si microscope with a Spectra Physics MaiTai laser. The image collection is done with nondescanned GaAsP detectors or a descanned spectral detector. The lens used for the acquisitions is a $25 \times W$ with a numerical aperture of 1.1. The excitation wavelength was fixed at 840 nm and all sample images were acquired with the same parameters (image size, detectors' gain and offset, and filters). The SHG signal was collected between 400 and 492 nm and the AF between 500 and 550 nm. For each sample, three stacks of images were acquired on a depth of around 40 μm. The pixel size was 0.21 μm and the z-step was 0.375 μm.

Because the section samples were not well flat and to only consider images with robust information, we selected the image slices with a sufficient mean intensity for the calculations. More precisely, I_{mean} being the mean intensity of a given slice and $I_{\max}$ being the mean intensity of the most intense slice of the 3-D stack, we applied the criterion $I_{\text{mean}} > 0.8 \times I_{\max}$ to only consider the most intense slices. The parameter calculations were performed on the selected 35 ± 5 slices, corresponding to a total depth of 13 ± 2 μm.

As for controlling the separability between SHG and AF signals, spectral images were also acquired between 400 and 650 nm with a spectral detector, with a resolution of 10 nm.

All images were acquired below the dermis–epidermis junction and were centered in the upper reticular dermis.

2.4 *First-Order Analysis*

All image analysis was performed with MATLAB (MathWorks, Natick, Massachusetts). Calculations were performed on the whole 3-D volume. A fixed threshold is applied, and the densities of collagen and elastin are calculated according to that threshold:

density: $\rho = \frac{N(I>400)}{N}$, where $N(I > 400)$ is the number of pixels with an intensity >400 and N is the total number of pixels.

Several statistical moments[18] and the entropy of the distribution[19] were calculated on the histograms:

mean intensity: $\mu = E[I]$,

standard deviation (STD): $\sigma = \sqrt{E[(I-\mu)^2]}$,

kurtosis: $K = E[(\frac{I-\mu}{\sigma})^4]$,

skewness: $S = E[(\frac{I-\mu}{\sigma})^3]$, and

entropy: $S = E[-\ln(p)]$,

where I is the histogram of intensities of the 3-D image, p is its probability mass function, and $E[.]$ is the expected value operator. Both parameters are calculated for SHG and AF signals.

2.5 *Wavelet Analysis*

In this part, maximum intensity projection (MIP) of 3-D images has been considered. The wavelet decomposition of the two-dimensional projections has been performed using Daubechies wavelet at the first scale.[14] Horizontal, vertical, and diagonal coefficients are then put in a single histogram, which can be modeled by a GGD:

$$f_{\alpha,\beta}(x) = \frac{\beta}{2\alpha\Gamma\left(\frac{1}{\beta}\right)} \exp\left[-\left(\frac{|x|}{\alpha}\right)^{\beta}\right],$$

where α and β are the scale and the shape parameters of the GGD, respectively, and $\Gamma(.)$ is the gamma function.

The parameters α and β are then used to characterize the images.

2.6 *Statistics*

For each parameter, a statistical analysis was made to determine the significance of the differences between zones and between groups. A Wilcoxon–Mann–Whitney test was done to compare values between groups and a paired Wilcoxon test to compare study areas inside each group. A p-value under 0.05 was considered significant.

3 Results

Typical acquisitions are shown in Figs. 1 and 2. Collagen fibers appear very dense and the collagen network cannot be visualized in great detail. On the contrary, elastin exhibits a strong AF, enabling a precise visualization of its fiber network. Nevertheless, we noticed that the elastin network on the forearm of the older group was different from all the other samples: elastin fibers were not well-defined and the elastin material appeared spread over the whole dermis.

3.1 *Spectral Analysis*

To confirm that SHG and AF signals can be accurately analyzed separately, multispectral images were acquired on different skin samples. Mean gray values were spectrally analyzed according to the wavelength. They exhibited a clear bimodal response (cf. Fig. 3). A sharp peak can be noticed at 420 nm, which corresponds to the SHG signal (the laser excitation wavelength being 840 nm). A second broad peak is observed between 450 and 550 nm, which corresponds to the AF signal. Both signals appear well-defined and clearly different from each other.

3.2 *Colocalization Analysis*

The first channel has a broad spectral detection windows (400 to 492 nm), which includes part of the AF signal. A colocalization

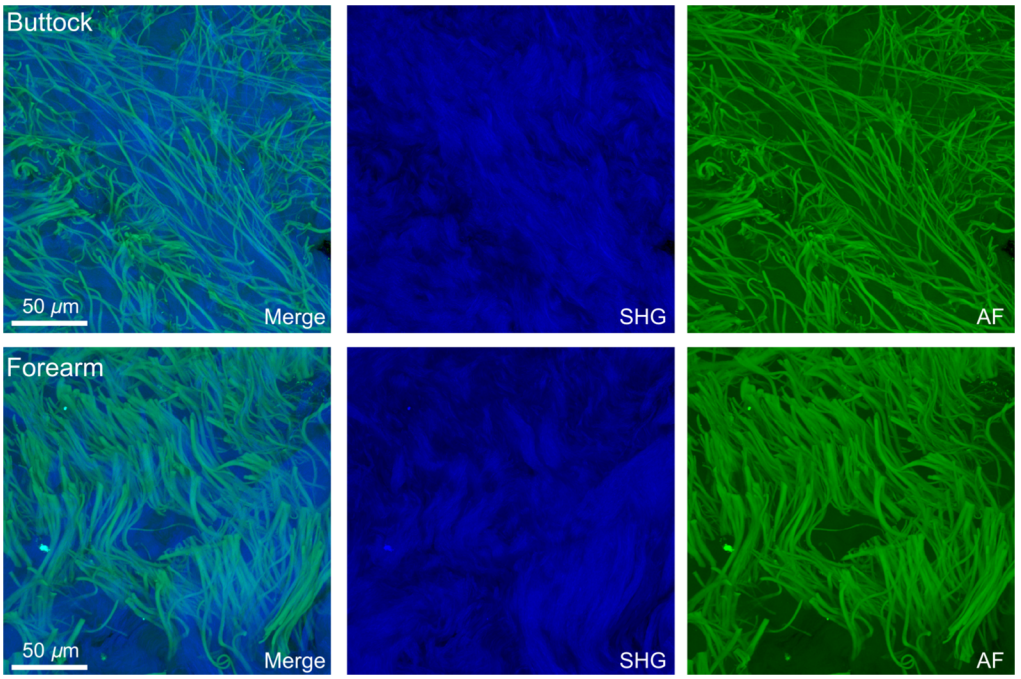

Fig. 1 MIP images of multiphoton acquisitions for a typical subject of the first group (aged 20 to 30). SHG, collagen fibers, and AF, elastin fibers.

analysis was performed between the "blue" and "green" channels to evaluate the independence of the two measured signals.

From Fig. 4, we observe two different signal dynamics. A Pearson correlation coefficient was computed for each acquisition and we obtained a mean coefficient of 0.13. This analysis showed that the two signals were not highly correlated. We can thus assess that the two signals are mostly independent and then attribute the blue channel primarily to collagen and the green channel primarily to elastin.

3.3 *First-Order Analysis*

The SAAID was calculated on MIP images (results are shown in Fig. 5). This parameter exhibited a clear difference between the older and younger skin ($p = 0.009$ and 0.015 on the buttock and

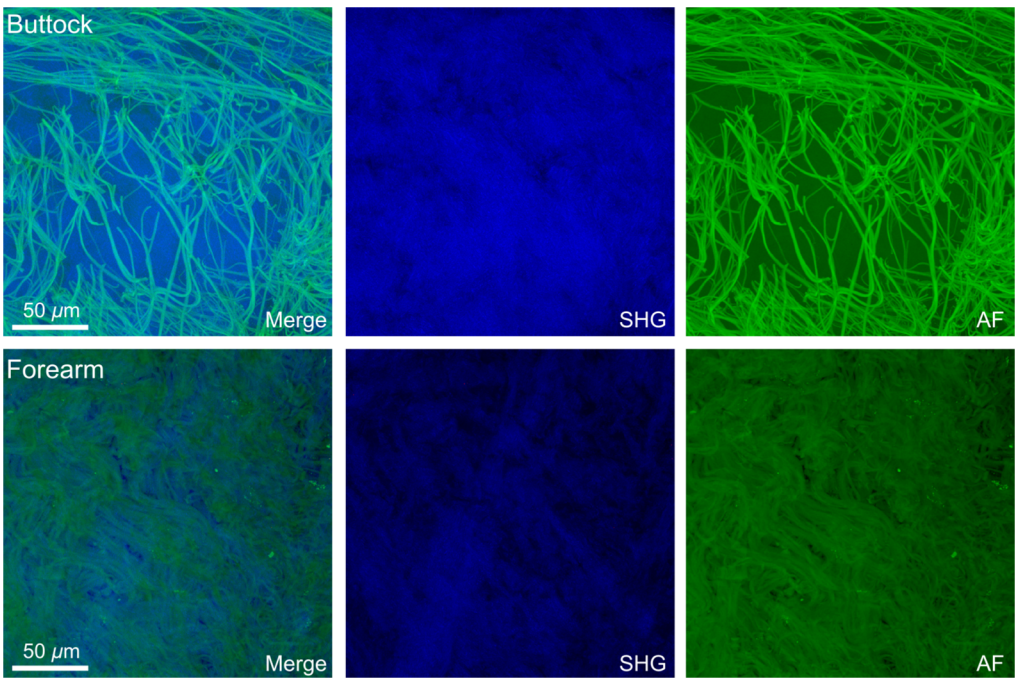

Fig. 2 MIP images of multiphoton acquisitions for a typical subject of the second group (aged 60 and older). SHG, collagen fibers, and AF, elastin fibers.

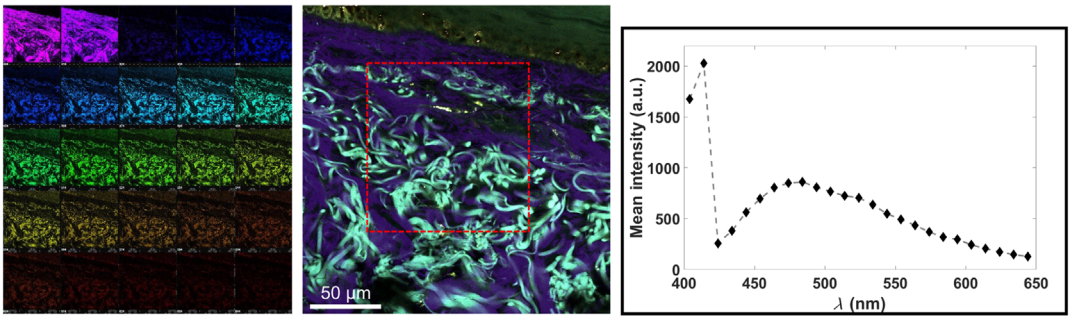

Fig. 3 Spectral analysis of the signal: (a) acquisition of the 25 images corresponding to 25 different wavelength bands, (b) color reconstruction of the signal and delineation of the region of interest, and (c) mean intensity value of the signal according to the wavelength.

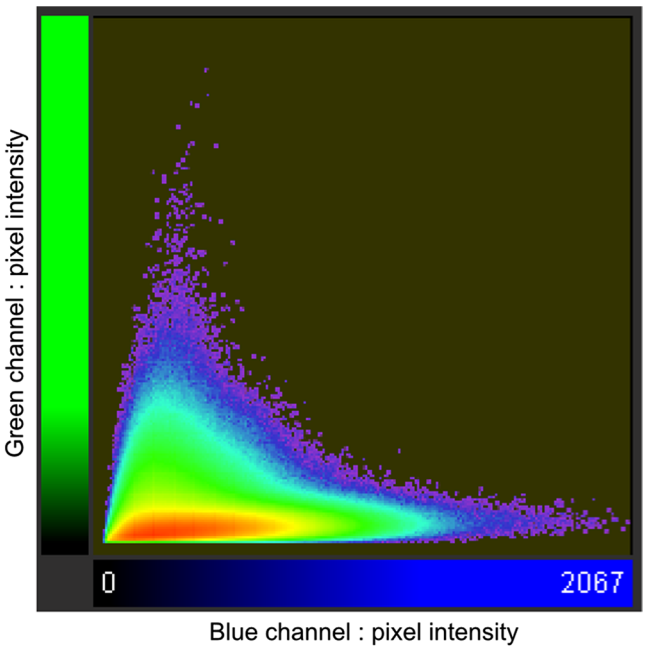

Fig. 4 Example of a colocalization histogram for one single acquisition.

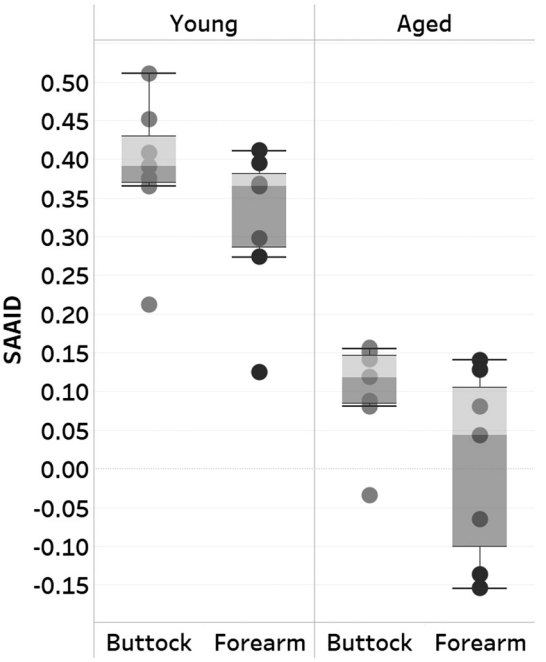

Fig. 5 SAAID values.

the forearm, respectively). Moreover, chronically UV-exposed older skin appeared more affected than the UV-protected skin (group 2, $p = 0.016$).

To precisely analyze the differences between intrinsic and extrinsic aging of the dermal fibers, SHG, and AF signals were also studied separately.

First-order parameters were calculated on the SHG images (cf. Fig. 6 and Appendix, Table 2 for statistical analysis). Mean intensity and skewness of the images' distributions were significantly different between the buttock and the forearm for both groups (group 1, $p = 0.016$ and 0.047 for mean intensity and skewness, respectively; group 2, $p = 0.016$ and 0.016 for mean intensity and skewness, respectively). We observed that the median intensity histograms (Fig. 7) exhibited a more compact distribution on the forearm, corresponding to a weaker SHG signal. We also observed that the density of collagen was significantly weaker on the forearm than on the buttock ($p = 0.016$ for group 1 and group 2). The collagen density and the SHG intensity tend to increase on the buttock whereas we see the opposite effects on the forearm. This could be explained by different mechanisms occurring in intrinsic and extrinsic aging.

The same parameters have been calculated on the AF signal that gives information on the presence of elastin in the dermis. Results are shown in Fig. 8 and complete statistical analysis in the Appendix (Table 3). We first notice that in the younger group, there are few differences between the AF signals on the buttock and on the forearm. Their histograms appear very similar (cf. Fig. 9) and only the mean intensity parameter exhibits a significant difference ($p = 0.0313$). The differences between groups are more significant: elastin occupies more space (higher density, $p = 0.019$ on the buttock), its intensity appears greater ($p = 0.024$ and 0.012 on the buttock and the forearm, respectively), and the signal has a higher entropy in the dermis of older skin ($p = 0.024$ on the buttock and the forearm).

These observations are in accordance with what we see in the images: the elastin network seems to be less organized in older skin and its fibers spread throughout the whole dermis.

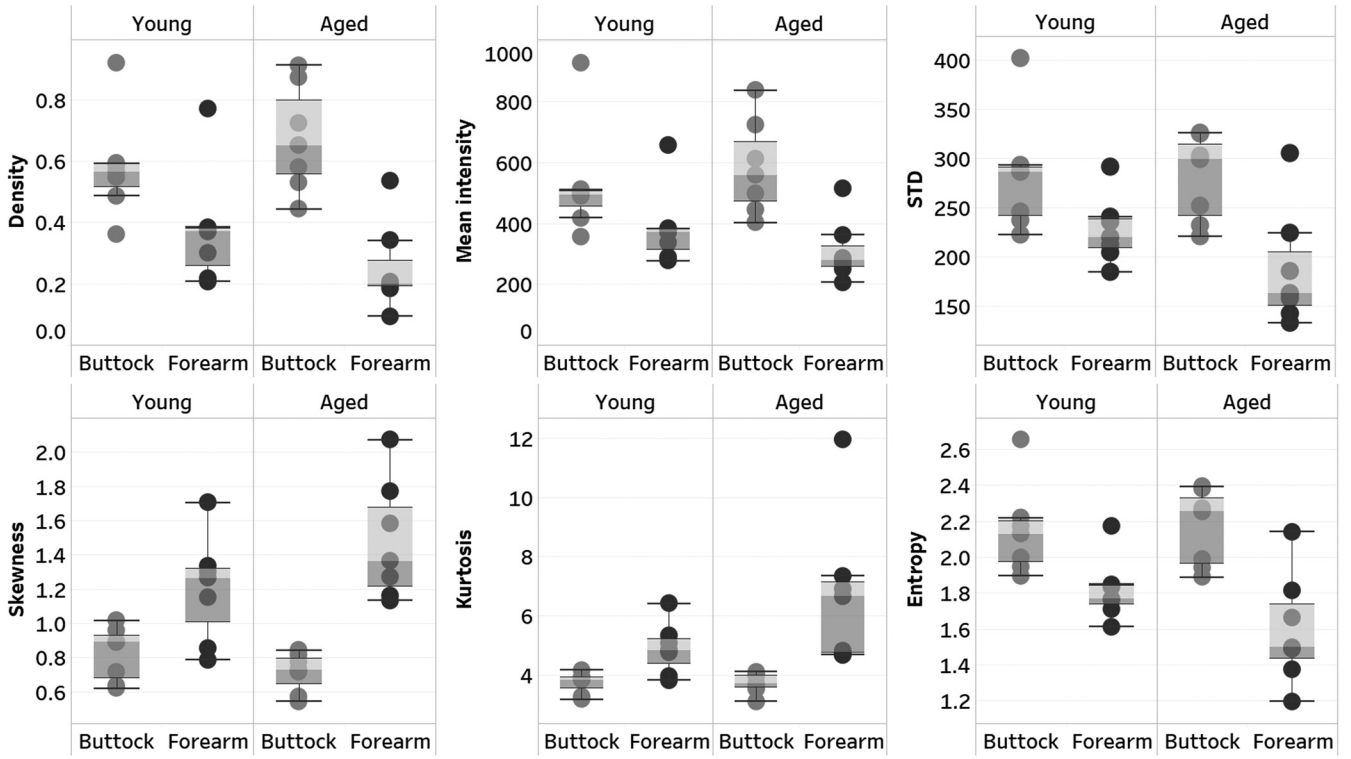

Fig. 6 First-order analysis of the SHG signal.

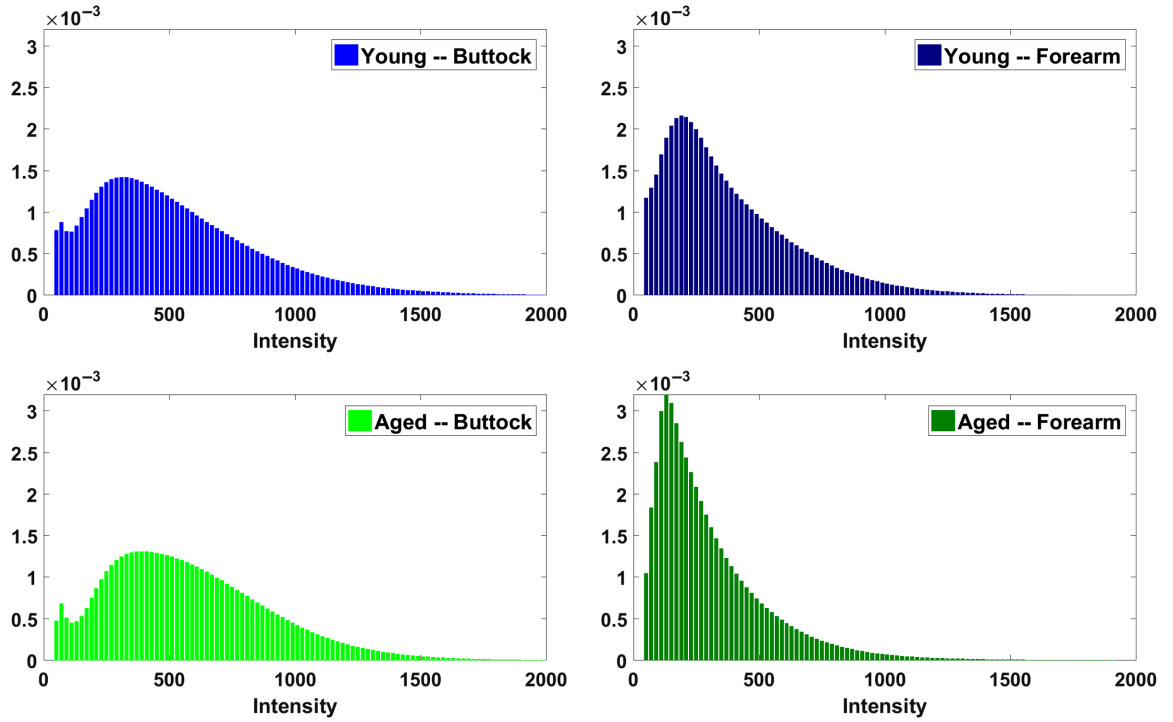

Fig. 7 Mean SHG intensity histograms for the two groups and the two zones.

Therefore, the images appear more homogeneous, in accordance with a lower entropy level. However, aging acts differentially on the buttock than on the forearm. Looking at the median histograms for the buttock (Fig. 9), the intensity distribution spreads with age. This leads to a higher proportion of high intensity pixels, corresponding to the well-defined elastin fibers. On the contrary, on the forearm, the intensity distribution exhibits a very thin tail, thus giving a large majority of low intensity pixels on the image. This is coherent with the fact that we observe very homogeneous texture on the older group forearm skin. Therefore, we observe different changes in elastin structure with intrinsic aging than with photoaging.

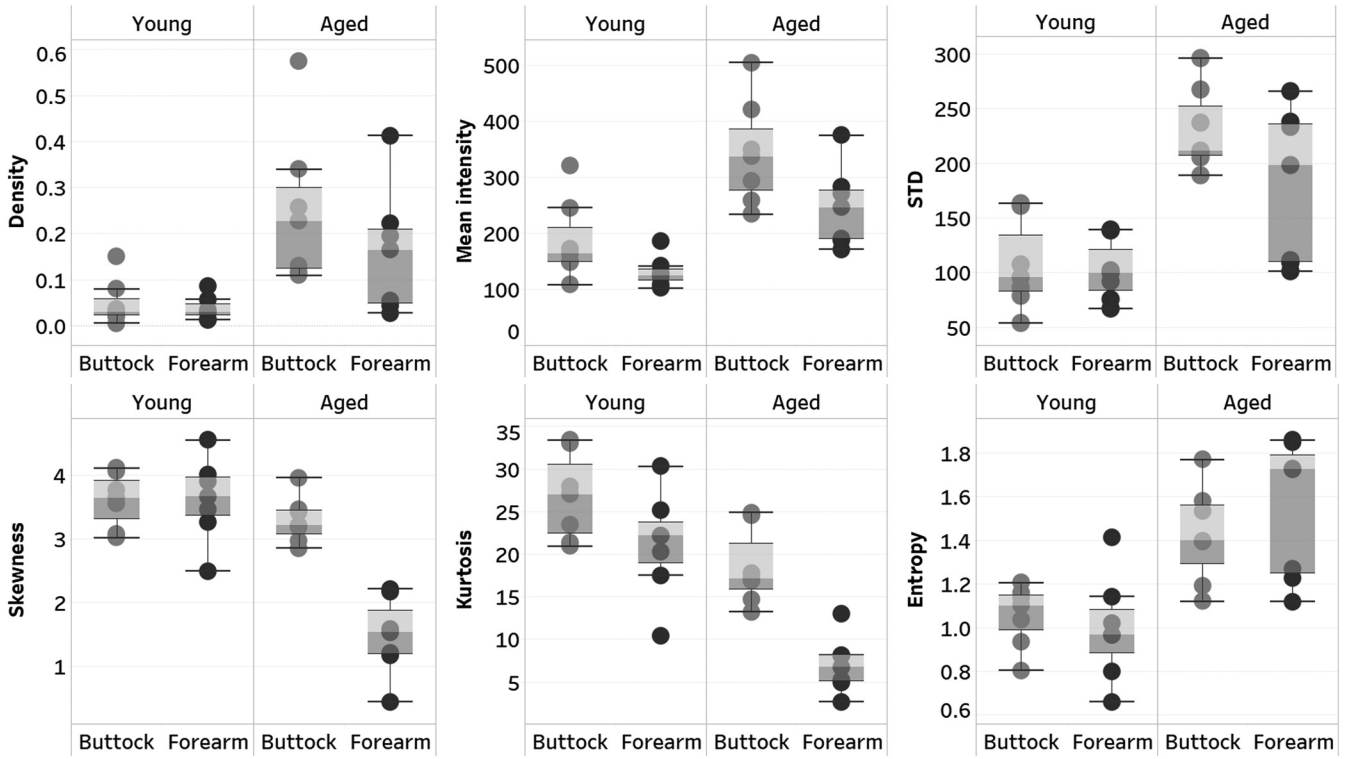

Fig. 8 First-order analysis of the AF signal.

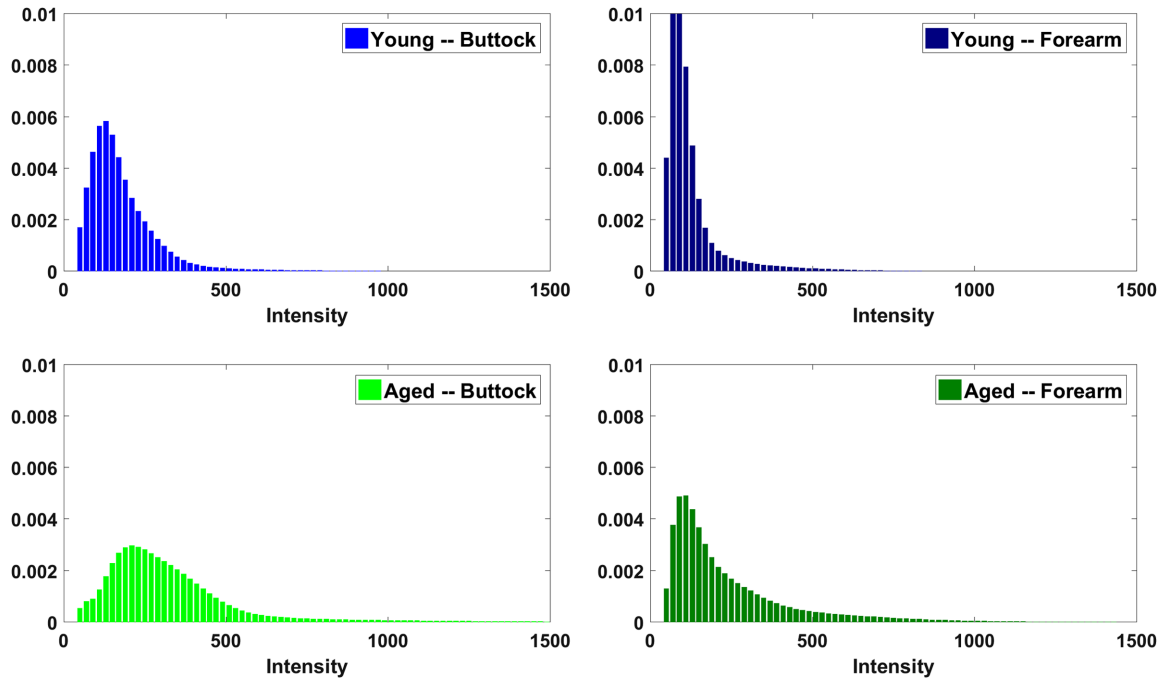

Fig. 9 Mean AF intensity histograms for the two groups and the two zones.

3.4 *Wavelet Analysis*

The analysis of the wavelet coefficients gives specific information about the images' texture. This analysis was performed on SHG and AF signals; the results are shown in Figs. 10 and 11 for the SHG signal and Figs. 12 and 13 for the AF signal. Statistical analysis is presented in the Appendix (Tables 4 and 5).

For the SHG signal, we observe larger differences between the two skin zones than between the two age groups, as was seen in the first-order analysis. Lower α and β parameters were measured on the buttock than on the forearm. The buttock skin area also presented a more compact wavelet coefficient distribution. This might reflect a lower diversity of textures as well as a lower prevalence of the most common collagen texture. No clear variations relative to aging were observed for these parameters.

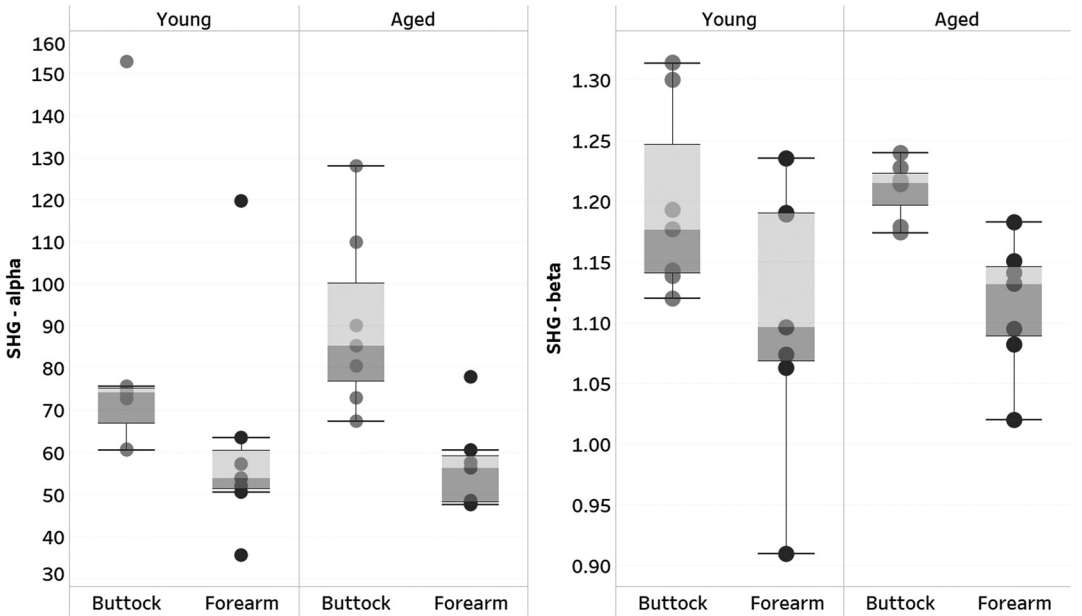

Fig. 10 Wavelet analysis on SHG images.

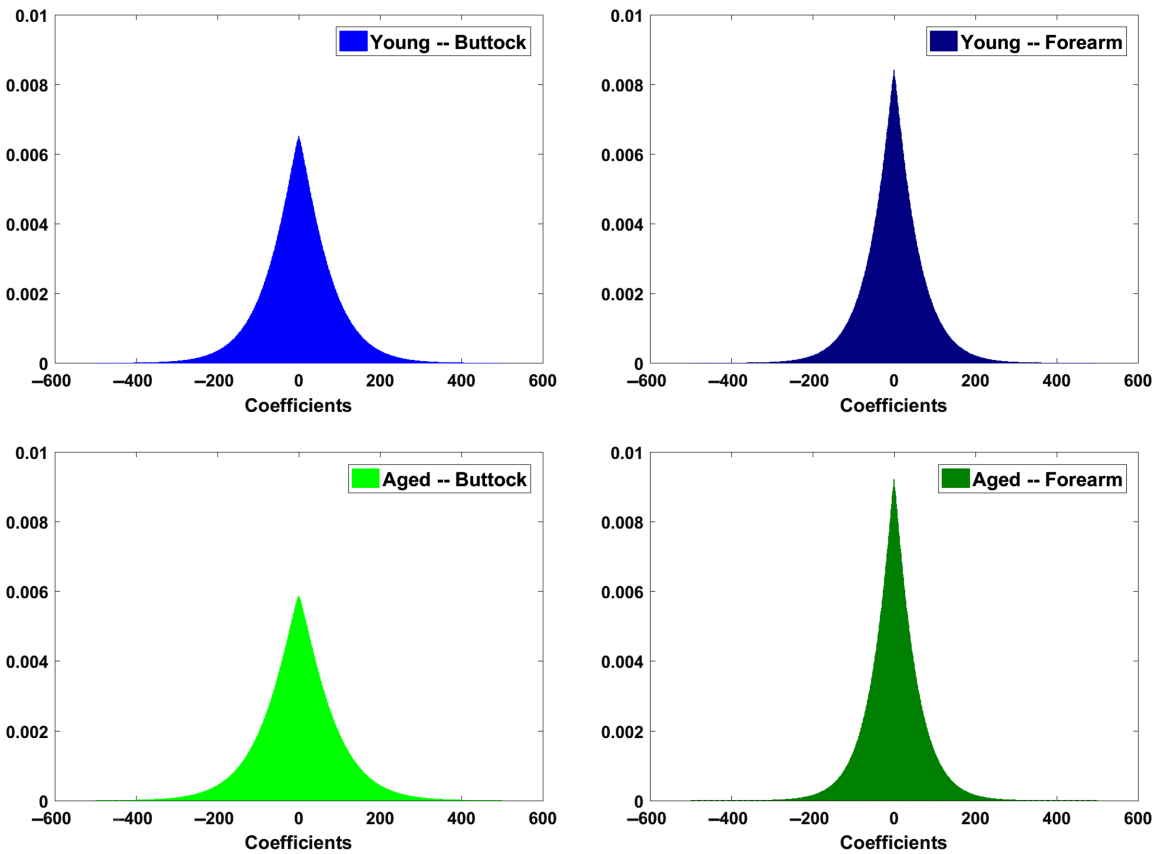

Fig. 11 GGD distributions generated with the mean α and β parameters calculated for SHG signal.

The AF signal exhibits a more complex response in regards to aging and photoaging. The α parameter increases with aging on both skin zones (comparison between groups: $p = 0.024$ on the buttock and $p = 0.031$ on the forearm). This scale parameter increase demonstrates the fact that the GGD distribution is more widely spread, and it also reflects the larger diversity of image textures.

The β value increases with aging only on the forearm skin area ($p = 0.039$). It thus appears to be modified by photoaging. An increase of this shape parameter means that the distribution is flatter for high wavelet coefficients, leading to lower variance and entropy of their distribution. Thus, the texture of the elastin network in the photoaged dermis is different from that observed on the other skin areas, as it is more homogeneous. The

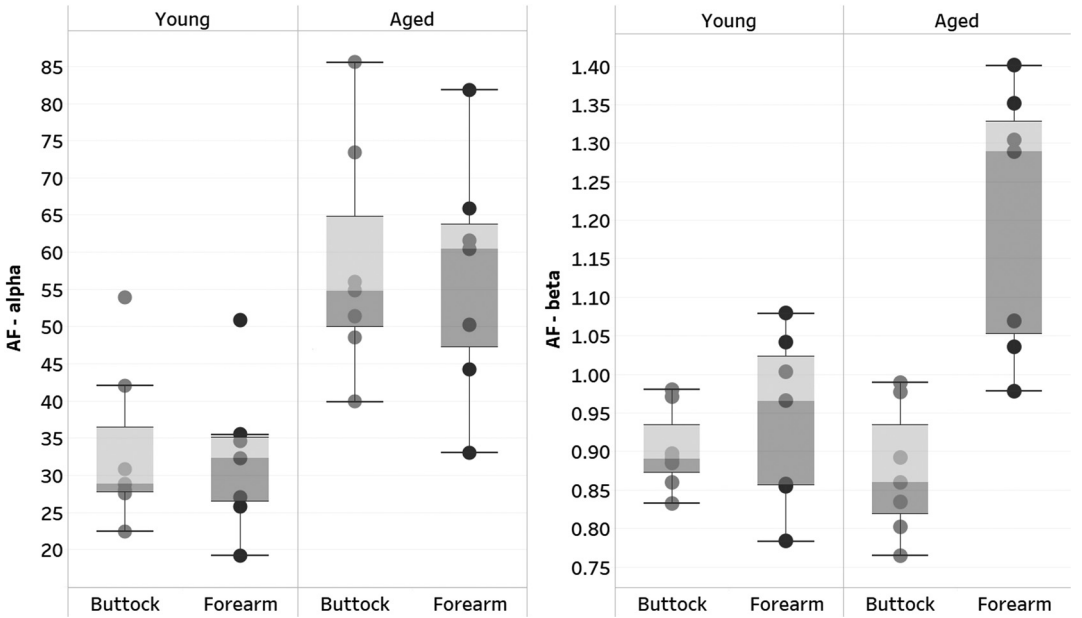

Fig. 12 Wavelet analysis on AF images.

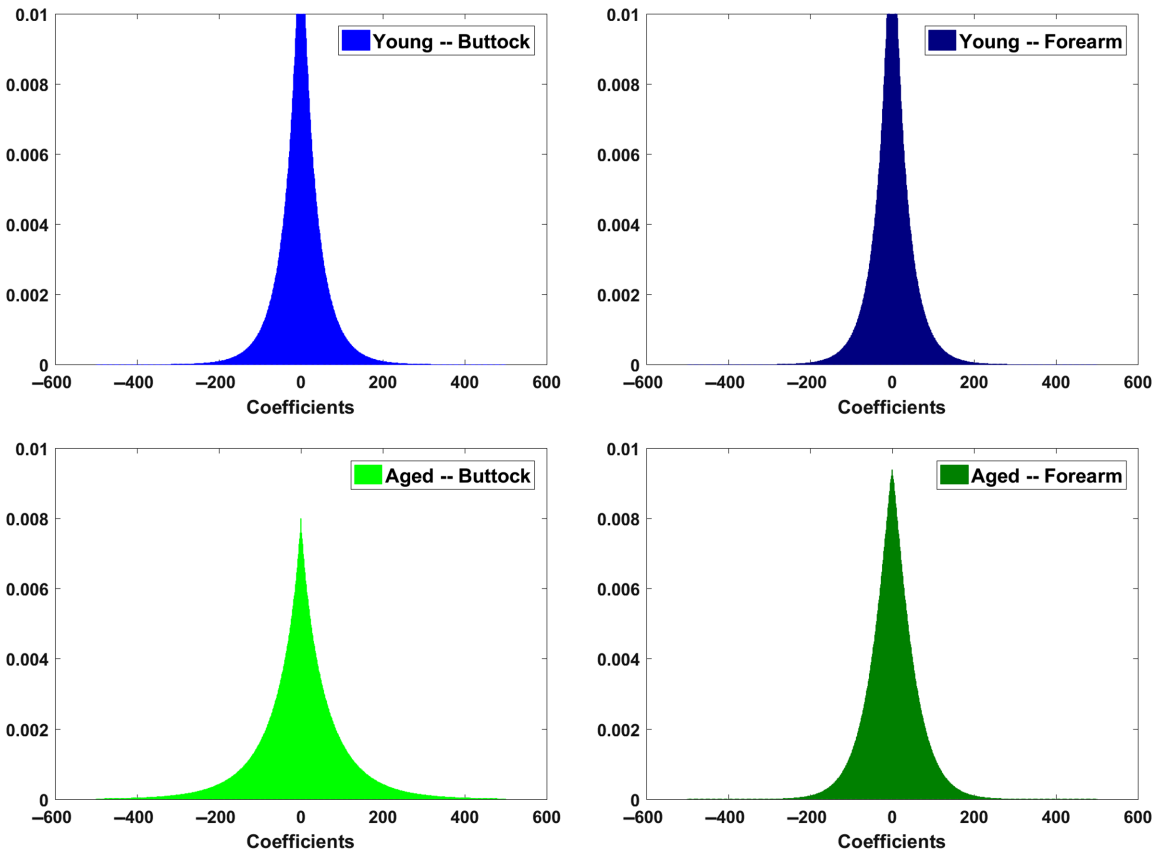

Fig. 13 GGD distributions generated with the mean α and β parameters calculated for AF signal.

combined increase of α and β implies a reduction in the texture variety.

4 Discussion

Collagen fibers organization appears different on the buttock and on the forearm. The latter shows a lower density and intensity of the SHG signal.

The collagen network appears more compact with aging. But the lower SHG signal measured on aged skin can also result from a higher cross-linking level as reported by Lutz et al.[20] With the wavelet analysis, we showed that the collagen network presents a lower diversity of textures on the forearm compared to the buttock. This can also be explained by the higher reticulation level, which decreases the fibers' motility. Differences in fibers

organization between these two skin zones could be caused by different types of mechanical stress. This stress has been shown to increase the production of elastic fibers.[21]

It is known that aging and photoaging may act through different mechanisms. Glycosaminoglycan (GAG) and hyaluronic acid (HA) concentrations in the dermis tend to decrease with intrinsic aging,[22] which in particular leads to a lower reticulation level of collagen, as these molecules help create bridges between collagen fibers. A lower level of reticulation leads to a more intense SHG signal as well as to greater collagen density, as the collagen network will occupy more space in the dermis.[20] On the contrary, photoaging provokes an increase of GAG and HA in the dermis. In this way, when we compare the SHG signal with aging on the buttock and the forearm, we observe opposite trends, as the buttock is a naturally photoprotected area whereas the forearm is chronically photoexposed.

Another important phenomenon to be considered is the increase of metalloproteinases (MMP), a protein able to degrade elastin fibers,[1] in the dermis of aging skin. This excess of MMP will generate more elastin fragments and reduce the number of large and well-defined fibers. Thus, the density of elastin increases as all these fragments occupy more space in the dermis and the number of different structures increases too, as we noticed with the growth of the α parameter (wavelet analysis). Nevertheless, the future of all these newly created elastin fragments will be different in intrinsic versus extrinsic aging. Solar elastosis, which has been well-documented, is characterized by an increase of elastin material in the upper dermis.[23,24] This phenomenon is specific to sun-damaged skin and is due to the binding of several molecules to the elastin fibers, which blocks elastolytic degradation.[25–27] Thereby, the large amount of elastin fragments caused by an excess of MMP leads to higher elastin content in the dermis of photoexposed skin, whereas on photoprotected skin these fragments are easily degraded. These combined mechanisms explain why we observe a prevalence of bigger elastin fibers on the photoprotected aged dermis, as the smaller fibers are more easily degraded. On the other hand, the texture on the photoexposed dermis is very homogeneous as all the elastin material remains without forming any structure. The first-order analysis and the wavelet analysis can capture these phenomena; some parameters are specific to intrinsic aging (density, intensity, and α) and others to extrinsic aging (STD and β).

Overall, more precise results and higher statistical significance were observed for the elastin analysis compared to collagen one. The collagen analysis may have suffered from the fact that a broad filter ($400 < \lambda < 492$ nm), which partially integrate AF signal was used on the blue channel. Instead, a very narrowband filter centered on the SHG wavelength would have been more selective. Nevertheless, this question is attenuated for the SAAID and wavelet analyses, which are performed on the MIP images. The MIP procedure selects the most intense signal, which is SHG in the blue channel.

5 Conclusion

Some parameters have been proposed for quantifying dermal aging,[4,6] but they do not provide any information about the collagen or elastin structures. We demonstrated that a systematic analysis of the SHG and AF signals can provide much information on the dermal matrix. A first-order analysis allows the evaluation of the density of collagen and elastin networks, and their homogeneity SHG signal intensity can be related to the collagen reticulation level. It appears that wavelet analysis can target different aging mechanisms of the elastin network in the dermis. This technique, which is specific to elastin, can discriminate intrinsic aging from solar elastosis and can provide a quantitative and objective value for aging. However, more analysis should be performed to identify if the α and β parameters can precisely capture different degrees of aging.

Appendix: Statistical Analysis

A Wilcoxon–Mann–Whitney test was done to compare values between groups and a paired Wilcoxon test to compare study areas inside each group. A p-value under 0.05 was considered significant (Tables 1–5).

Table 1 SAAID statistical analysis.

Comparison	p-value	Significance
Group 1: difference between sites	0.0469	S
Group 2: difference between sites	0.0156	S
Buttock: difference between groups	0.0090	S
Forearm: difference between groups	0.0147	S

Table 2 Statistical analysis of the first-order analysis on SHG signal.

Parameter	Comparison	p-value	Significance
Density	Group 1: difference between sites	0.0156	S
	Group 2: difference between sites	0.0156	S
	Buttock: difference between groups	0.4570	NS
	Forearm: difference between groups	0.0970	NS
Intensity	Group 1: difference between sites	0.0156	S
	Group 2: difference between sites	0.0156	S
	Buttock: difference between groups	0.4570	NS
	Forearm: difference between groups	0.1206	NS

Table 2 (*Continued*).

Parameter	Comparison	*p*-value	Significance
STD	Group 1: difference between sites	0.0313	S
	Group 2: difference between sites	0.0781	NS
	Buttock: difference between groups	0.7077	NS
	Forearm: difference between groups	0.1492	NS
Skewness	Group 1: difference between sites	0.0469	S
	Group 2: difference between sites	0.0156	S
	Buttock: difference between groups	0.2709	NS
	Forearm: difference between groups	0.2237	NS
Kurtosis	Group 1: difference between sites	0.0313	S
	Group 2: difference between sites	0.0156	S
	Buttock: difference between groups	1	NS
	Forearm: difference between groups	0.2237	NS
Entropy	Group 1: difference between sites	0.0156	S
	Group 2: difference between sites	0.0156	S
	Buttock: difference between groups	0.8023	NS
	Forearm: difference between groups	0.1206	NS

Table 3 Statistical analysis of the first-order analysis on AF signal.

Parameter	Comparison	*p*-value	Significance
Density	Group 1: difference between sites	0.4688	NS
	Group 2: difference between sites	0.1563	NS
	Buttock: difference between groups	0.0188	S
	Forearm: difference between groups	0.0775	NS

Table 3 (*Continued*).

Parameter	Comparison	*p*-value	Significance
Intensity	Group 1: difference between sites	0.0313	S
	Group 2: difference between sites	0.0156	S
	Buttock: difference between groups	0.0239	S
	Forearm: difference between groups	0.0115	S
STD	Group 1: difference between sites	0.5781	NS
	Group 2: difference between sites	0.2188	NS
	Buttock: difference between groups	0.0090	S
	Forearm: difference between groups	0.0489	S
Skewness	Group 1: difference between sites	1	NS
	Group 2: difference between sites	0.0156	S
	Buttock: difference between groups	0.1833	NS
	Forearm: difference between groups	0.0090	S
Kurtosis	Group 1: difference between sites	0.1094	NS
	Group 2: difference between sites	0.0156	S
	Buttock: difference between groups	0.0387	S
	Forearm: difference between groups	0.0115	S
Entropy	Group 1: difference between sites	0.6875	NS
	Group 2: difference between sites	0.5781	NS
	Buttock: difference between groups	0.0239	S
	Forearm: difference between groups	0.0239	S

Table 4 Statistical analysis of the wavelet parameters calculated on SHG signal.

Parameter	Comparison	*p*-value	Significance
α	Group 1: difference between sites	0.0313	S
	Group 2: difference between sites	0.0156	S
	Buttock: difference between groups	0.2237	NS
	Forearm: difference between groups	0.9003	NS
β	Group 1: difference between sites	0.1563	NS
	Group 2: difference between sites	0.0156	S
	Buttock: difference between groups	0.3874	NS
	Forearm: difference between groups	0.9003	NS

Table 5 Statistical analysis of the wavelet parameters calculated on AF signal.

Parameter	Comparison	*p*-value	Significance
α	Group 1: difference between sites	0.6875	NS
	Group 2: difference between sites	0.9375	NS
	Buttock: difference between groups	0.0239	S
	Forearm: difference between groups	0.0305	S
β	Group 1: difference between sites	0.3750	NS
	Group 2: difference between sites	0.0156	S
	Buttock: difference between groups	0.6178	NS
	Forearm: difference between groups	0.0387	S

Disclosures

The authors have no relevant financial interests in this article and no potential conflicts of interest to disclose.

Acknowledgments

We thank Emmanuel Questel and Anne-Lise Bardy (Pierre Fabre Dermo Cosmétique, Toulouse, France) for the clinical study management and fulfilment.

References

1. A. K. Langton et al., "A new wrinkle on old skin: the role of elastic fibres in skin ageing," *Int. J. Cosmet. Sci.* **32**(5), 330–339 (2010).
2. P. J. Campagnola and L. M. Loew, "Second-harmonic imaging microscopy for visualizing biomolecular arrays in cells, tissues and organisms," *Nat. Biotechnol.* **21**(11) 1356–1360 (2003).
3. A. Zoumi et al., "Imaging coronary artery microstructure using second-harmonic and two-photon fluorescence microscopy," *Biophys. J.* **87**(4), 2778–2786 (2004).
4. M. J. Koehler et al., "*In vivo* assessment of human skin aging by multiphoton laser scanning tomography," *Opt. Lett.* **31**(19), 2879–2881 (2006).
5. K. Sugata et al., "Evaluation of photoaging in facial skin by multiphoton laser scanning microscopy," *Skin Res. Technol.* **17**(1), 1–3 (2011).
6. S. Puschmann et al., "Approach to quantify human dermal skin aging using multiphoton laser scanning microscopy," *J. Biomed. Opt.* **17**(3), 036005 (2010).
7. J. C. Pittet et al., "Evaluation of elastin/collagen content in human dermis in-vivo by multiphoton tomography—variation with depth and correlation with aging," *Cosmetics* **1**(3), 211–221 (2014).
8. R. Cicchi et al., "Scoring of collagen organization in healthy and diseased human dermis by multiphoton microscopy," *J. Biophotonics* **3**(1–2), 34–43 (2010).
9. S. Wu et al., "Quantitative analysis on collagen morphology in aging skin based on multiphoton microscopy," *J. Biomed. Opt.* **16**(4), 040502 (2011).
10. J. S. Bredfeldt et al., "Computational segmentation of collagen fibers from second-harmonic generation images of breast cancer," *J. Biomed. Opt.* **19**(1), 016007 (2014).
11. A. C. Weihermann et al., "Elastin structure and its involvement in skin photoageing," *Int. J. Cosmet. Sci.* **39**(3), 241–247 (2017).
12. M. C. Hughes et al., "Comparison of histological measures of skin photoaging," *Dermatology* **223**(2), 140–151 (2011).
13. P. L. Tong et al., "A quantitative approach to histopathological dissection of elastin-related disorders using multiphoton microscopy," *Br. J. Dermatol.* **169**(4), 869–879 (2013).
14. I. Daubechies, *Ten Lectures on Wavelets*, Society for Industrial and Applied Mathematics, Philadelphia, Pennsylvania (1992).
15. M. N. Do and M. Vetterli, "Wavelet-based texture retrieval using generalized Gaussian density and Kullback–Leibler distance," *IEEE Trans. Image Process.* **11**(2), 146–158 (2002).
16. A. Halimi et al., "Wavelet-based statistical classification of skin images acquired with reflectance confocal microscopy," *Biomed. Opt. Express* **8**(12), 5450–5467 (2017).
17. A. Vierkötter et al., "The SCINEXA: a novel, validated score to simultaneously assess and differentiate between intrinsic and extrinsic skin ageing," *J. Dermatol. Sci.* **53**(3), 207–211 (2009).
18. R. C. Gonzalez and R. E. Woods, *Digital Image Processing*, 2nd ed., Pearson Education, Upper Saddle River, New Jersey (2002).
19. C. E. Shannon, "A mathematical theory of communication," *Bell Syst. Tech. J.* **27**, 379–423 (1948).
20. V. Lutz et al., "Impact of collagen crosslinking on the second harmonic generation signal and the fluorescence lifetime of collagen autofluorescence," *Skin Res. Technol.* **18**(2), 168–179 (2012).
21. E. Caberlotto et al., "Effects of a skin-massaging device on the ex-vivo expression of human dermis proteins and in-vivo facial wrinkles," *PLoS One* **12**(3), e0172624 (2017).
22. D. H. Lee, J. H. Oh, and J. H. Chung, "Glycosaminoglycan and proteoglycan in skin aging," *J. Dermatol. Sci.* **83**(3), 174–181 (2016).
23. J. Uitto, "The role of elastin and collagen in cutaneous aging: intrinsic aging versus photoexposure," *J. Drugs Dermatol.* **7**(2 Suppl.), s12–s16 (2008).
24. E. F. Bernstein and J. Uitto, "The effect of photodamage on dermal extracellular matrix," *Clin. Dermatol.* **14**(2), 143–151 (1996).

25. J. Muto et al., "Accumulation of elafin in actinic elastosis of sun-damaged skin: elafin binds to elastin and prevents elastolytic degradation," *J. Invest. Dermatol.* **127**(6), 1358–1366 (2007).
26. E. Yoshinaga et al., "$N(\varepsilon)$-(carboxymethyl)lysine modification of elastin alters its biological properties: implications for the accumulation of abnormal elastic fibers in actinic elastosis," *J. Invest. Dermatol.* **132**(2), 315–323 (2012).
27. S. Seite et al., "Elastin changes during chronological and photo-ageing: the important role of lysozyme," *J. Eur. Acad. Dermatol. Venereol.* **20**(8), 980–987 (2006).

Jimmy Le Digabel received his PhD in biophysics from Paris Diderot University in 2012. Currently, he is working in the R&D Department of Pierre Fabre Laboratories as a biophysics and imaging expert for clinical applications.

Sophia Houriez-Gombaud-Saintonge is currently a PhD student at Sorbonne University in the medical imaging field. She received her BSc and MSc degrees in electronic and signal processing engineering, with a specialization in image processing in 2016 from INP-ENSEEIHT.

Jérôme Filiol received his BSc degree in physiology and pharmacology from Nottingham Trent University in 1999. Since 2001, he is working in the R&D Department of Pierre Fabre Laboratories as biochemistry, bio-physics and imaging technician.

Christophe Lauze received a BSc degree in population genetics in 1991 and a MSc degree in statistics of life sciences and health in 1993 from Montpellier-II University. Currently, he is working in the R&D Department of Pierre Fabre Laboratories as a biostatistician for the analysis of clinical trials.

Gwendal Josse received his PhD of liquid physics from Pierre and Marie Curie University, Paris, in 2001. Since 2003, he has performed research on biomedical imaging in the Pierre Fabre Laboratories, where he is responsible for the bio-physics and imaging team.